CORONAVIRUS

Naive human B cells engage the receptor binding domain of SARS-CoV-2, variants of concern, and related sarbecoviruses

Jared Feldman[1]†, Julia Bals[1]†, Clara G. Altomare[2], Kerri St. Denis[1], Evan C. Lam[1], Blake M. Hauser[1], Larance Ronsard[1], Maya Sangesland[1], Thalia Bracamonte Moreno[1], Vintus Okonkwo[1], Nathania Hartojo[1], Alejandro B. Balazs[1], Goran Bajic[2], Daniel Lingwood[1]*, Aaron G. Schmidt[1,3]*

Initial exposure to a pathogen elicits an adaptive immune response to control and eradicate the threat. Interrogating the abundance and specificity of the naive B cell repertoire drives understanding of how to mount protective responses. Here, we isolated naive B cells from eight seronegative human donors targeting the severe acute respiratory syndrome coronavirus 2 (SARS-CoV-2) receptor binding domain (RBD). Single-cell B cell receptor (BCR) sequencing identified diverse gene usage and no restriction on complementarity determining region length. A subset of recombinant antibodies produced by naive B cell precursors bound to SARS-CoV-2 RBD and engaged circulating variants including B.1.1.7, B.1.351, and B.1.617.2, as well as preemergent bat-derived coronaviruses RaTG13, SHC104, and WIV1. By structural characterization of a naive antibody in complex with SARS-CoV-2 spike, we identified a conserved mode of recognition shared with infection-induced antibodies. We found that representative naive antibodies could signal in a B cell activation assay, and by using directed evolution, we could select for a higher-affinity RBD interaction, conferred by a single amino acid change. The minimally mutated, affinity-matured antibodies also potently neutralized SARS-CoV-2. Understanding the SARS-CoV-2 RBD–specific naive repertoire may inform potential responses capable of recognizing future SARS-CoV-2 variants or emerging coronaviruses, enabling the development of pan-coronavirus vaccines aimed at engaging protective germline responses.

INTRODUCTION

Initial exposure to viral antigens by natural infection or vaccination primes an immune response and often establishes immune memory, which can prevent or control future infections. The naive repertoire contains potential B cell receptor (BCR) rearrangements capable of recognizing these antigens, which are often surface-exposed glycoproteins. An early step in generating humoral immunity involves activation of these naive B cells through recognition of a cognate antigen (1), which, in turn, can lead to affinity maturation through somatic hypermutation (SHM) and subsequent differentiation (2). The initial engagement of the naive repertoire begins this cascade and often coincides with the eventual generation of a protective or neutralizing antibody response (3).

For severe acute respiratory syndrome coronavirus 2 (SARS-CoV-2), the etiological agent of coronavirus disease 2019 (COVID-19), the development of a neutralizing antibody response after primary infection or vaccination is associated with protection against reinfection in nonhuman primates (4, 5). In humans, the presence of neutralizing antibodies can predict disease severity and survival after primary SARS-CoV-2 infection (6) or vaccination (7). Furthermore, the two arms of humoral immune memory, long-lived bone marrow plasma cells (8) and circulating memory B cells (9, 10), are induced by natural infection in humans and may persist for at least 8 months after primary infection, providing potentially durable long-term protection. Comparable levels of neutralizing antibody titers are present in convalescent COVID-19 individuals and vaccine recipients (11), further supporting the role of adaptive immune responses in helping to control and prevent disease severity.

Both infection- and vaccine-elicited antibodies predominantly target the major SARS-CoV-2 envelope glycoprotein, spike, present on the virion surface. A substantial component of the neutralizing response engages the receptor binding domain (RBD) and does so by directly blocking interactions with angiotensin-converting enzyme 2 (ACE2), the host receptor for viral entry (12). Isolated RBD-directed monoclonal antibodies are derived from diverse heavy and light chain variable gene segments, suggesting that multiple biochemical solutions for developing RBD-directed antibodies are encoded within the human B cell repertoire (13, 14). Potential immunogenicity of this antigenic site is based on the human naive B cell repertoire and the overall frequency of naive BCRs that have some level of intrinsic affinity to stimulate their elicitation (15–17). However, antigen specificity of naive B cells is largely undefined.

Traditional approaches for studying antigen-specific naive B cells include bioinformatic mining of available BCR datasets and inference of likely germline precursors by "germline-reverting" mature BCR sequences. This can be limited by the availability of heavy and light chain paired sequence data and unreliable complementarity determining region 3 (CDR3) loop approximation, respectively. Here, we address this limitation by characterizing human naive B cells specific for the SARS-CoV-2 RBD directly from the peripheral blood of seronegative donors to understand their relative abundance, intrinsic affinity, and potential for activation. Furthermore, we asked whether the SARS-CoV-2–specific naive repertoire could also engage related circulating variants of concern and prepandemic

[1]Ragon Institute of MGH, MIT and Harvard, Cambridge, MA 02139, USA. [2]Department of Microbiology, Icahn School of Medicine at Mount Sinai, New York, NY 10029, USA. [3]Department of Microbiology, Harvard Medical School, Boston, MA 02115, USA.
*Corresponding author. Email: dlingwood@mgh.harvard.edu (D.L.); aschmidt@crystal.harvard.edu (A.G.S.)
†These authors contributed equally to this work.

CoVs. We find that SARS-CoV-2 RBD–specific naive B cells were of unrestricted gene usage and several isolated B cells had affinity for circulating SARS-CoV-2 variants and related CoV RBDs. We determined the structure of a representative naive antibody that binds the SARS-CoV-2 RBD with a mode of recognition similar to a multidonor class of antibodies prevalent in human responses to SARS-CoV-2 infection. Furthermore, we improved the affinity of two representative naive antibodies for RBD and showed that the starting naive specificity dictated the breadth of evolved clones to circulating variants. The analysis of the human naive antigen-specific B cell repertoire for the SARS-CoV-2 RBD and its capacity to recognize related variants and emerging CoVs may inform the rational design of epitope-focused immunogens for next-generation vaccines.

RESULTS

Isolated SARS-CoV-2–specific naive B cells are genetically diverse

To measure the reactivity of naive human B cells specific for the SARS-CoV-2 RBD, we adapted an ex vivo B cell profiling approach used previously to study epitope-specific naive precursors targeting neutralizing sites on HIV-1 (18) and influenza virus surface glycoproteins (15). We designed a SARS-CoV-2 RBD construct that positions two glycans at residues 475 and 501 to selectively block binding to ACE2 and the receptor binding motif (RBM)–directed antibody, B38 (fig. S1) (19). Using this "ΔRBM" probe, in addition to wild-type SARS-CoV-2 spike, and RBD probes, we isolated naive [CD19⁺/immunoglobulin D⁺ (IgD⁺)/IgG⁻] B cells specific to the RBD and, more finely, the RBM from the peripheral blood of eight SARS-CoV-2 seronegative human donors (Fig. 1A and fig. S1E). We defined RBM specificity as B cells that bound to fluorescently labeled spike and RBD, but not the ΔRBM probe (fig. S2A). Although rare, all eight donors had detectable populations of RBM-specific naive B cells (fig. S2B). The median frequency of RBM-specific B cells among total and naive B cells was 0.0025 and 0.0029%, respectively (Fig. 1B). Within spike-reactive naive cells, the median frequency of RBM-specific B cells was 3.6% (Fig. 1C). This suggests that a large proportion of spike epitopes targeted by naive responses reside outside of the RBD. Although different flow cytometric probes were used, recent studies suggest that the frequency of RBD-specific B cells in convalescent and vaccinated individuals may increase about 10-fold upon exposure to antigen (11). Furthermore, most of the IgD⁺ RBM-specific B cells were CD27⁻ (mean frequency ~97%), in agreement with the naive B cell phenotype (fig. S2C).

To understand in more detail the properties of this naive repertoire, we obtained 163 paired heavy and light chain antibody sequences from five of the eight donors. Sequence analysis showed
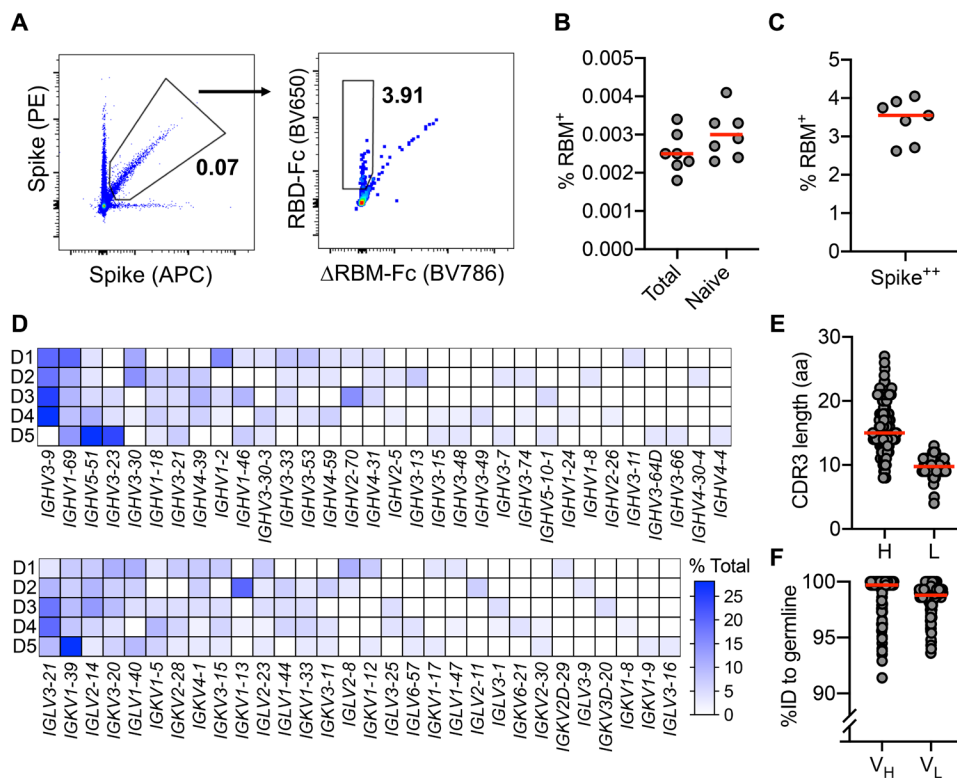

Fig. 1. SARS-CoV-2–specific naive B cell isolation and characterization. (**A**) RBM-specific naive B cells from seronegative human donors were isolated by FACS gated on CD19⁺IgD⁺IgG⁻; representative plot from donor 6 is shown. ΔRBM is a sorting probe with N-linked glycans at residues 501 and 475. RBM-specific B cell frequency among (**B**) total, naive, and (**C**) spike-positive cells from each donor (*n* = 7). Red bars indicate the mean percent values. (**D**) Heat map showing variable gene usage for all paired B cell sequences. Scale indicates percent of total sequences for each donor (D1 to D5). (**E**) Heavy (H) and light (L) CDR3 amino acid (aa) length distribution determined using IMGT numbering. Red bars indicate median amino acid length. (**F**) Divergence from inferred germline gene sequences. Red bars indicate the mean percent values. ID, identity.

that all clones were unique with diverse gene usage for both heavy and light chains, and minimal gene pairing preferences (Fig. 1D). These data reflect the polyclonal gene usage observed in RBD-specific memory B cells sequenced from COVID-19 convalescent individuals (13, 14) and vaccine recipients (11), suggesting that a diverse pool of antibody precursors can be activated upon antigen exposure. By comparing this naive repertoire with gene usage distribution from non–SARS-CoV-2–specific repertoires (20), we observed an increase in mean repertoire frequency of ~20% for IGHV3-9 in four of the five sequenced donors (fig. S3A). This enrichment of IGHV3-9 was also observed in isolated memory B cells from convalescent individuals (21) and vaccine recipients (11), as well as in expanded IgG⁺ B cells sequenced from a cohort of COVID-19 individuals during acute infection (22). These expanded clones, detected shortly after onset of symptoms, displayed low levels of SHM, suggesting potential IGHV3-9 usage in an early extrafollicular response in which naive B cells differentiate into short-lived plasma cells (23). In addition, IGHV3-53 and IGHV3-30 gene segments, overrepresented in RBD-specific antibodies isolated from convalescent individuals (24), were recovered from three sequenced donors (13 total clones; ~8.0% of the total). The amino acid length of heavy and light chain third CDR3 ranged from 8 to 27 (average length, ~16) for HCDR3 and 4 to 13 (average length, ~10) for LCDR3 (Fig. 1E). These lengths are normally

distributed relative to both unselected human repertoires (*20*) and RBD-specific memory B cell repertoires (*24*). These data suggest that overall HCDR3 length does not restrict precursor frequency and that there appears no inherent bias for CDR3 length conferring RBM specificity. Most of the obtained sequences were at germ line in both the variable heavy (V_H) and light (V_L) chains. However, despite sorting B cells with a naive phenotype, some sequences were recovered that deviated from germ line. Specifically, the V_H ranged from 91.4 to 100% identity to germ line, with a median of 99.7%; the V_L ranged from 93.6 to 100%, with a median of 99.3% (Fig. 1F and fig. S2, B and C).

Naive antibodies engage SARS-CoV-2 RBD with high affinity
To obtain affinities of the isolated naive antibodies, we cloned and recombinantly expressed 38 IgG antibodies selected to reflect the polyclonal RBD-specific repertoire with representatives from diverse variable region gene segments and 32 unique heavy chain–light chain

pairings (table S1). In addition, we ensured diversity in terms of HCDR3 length, kappa and lambda usage, and representation from all five donors. By enzyme-linked immunosorbent assay (ELISA), we identified IgGs with detectable binding to SARS-CoV-2 RBD; we summarize these results for all antibodies (Fig. 2A) and parsed by donor (fig. S3D). Across 5 donors, 33 (~87%) bound to monomeric SARS-CoV-2 RBD (Fig. 2A), with median effective concentration (EC_{50}) values ranging from 3.3 to 410 nM and a mean of 59 nM (Fig. 2A and fig. S3E). Of the binding population, there was no apparent predisposition for HCDR3 length or light chain pairing (Fig. 2, C and D). We further defined the epitopic region of these IgGs using the ΔRBM construct and the individual glycan variants, Δ501 and Δ475, both of which independently block ACE2 cell surface binding but are on opposite sides of the RBM (fig. S1, E and F). Nine IgGs had no detectable ΔRBM binding (e.g., ab079 and ab119), whereas 20 IgGs had reduced ELISA binding relative to wild-type RBD,
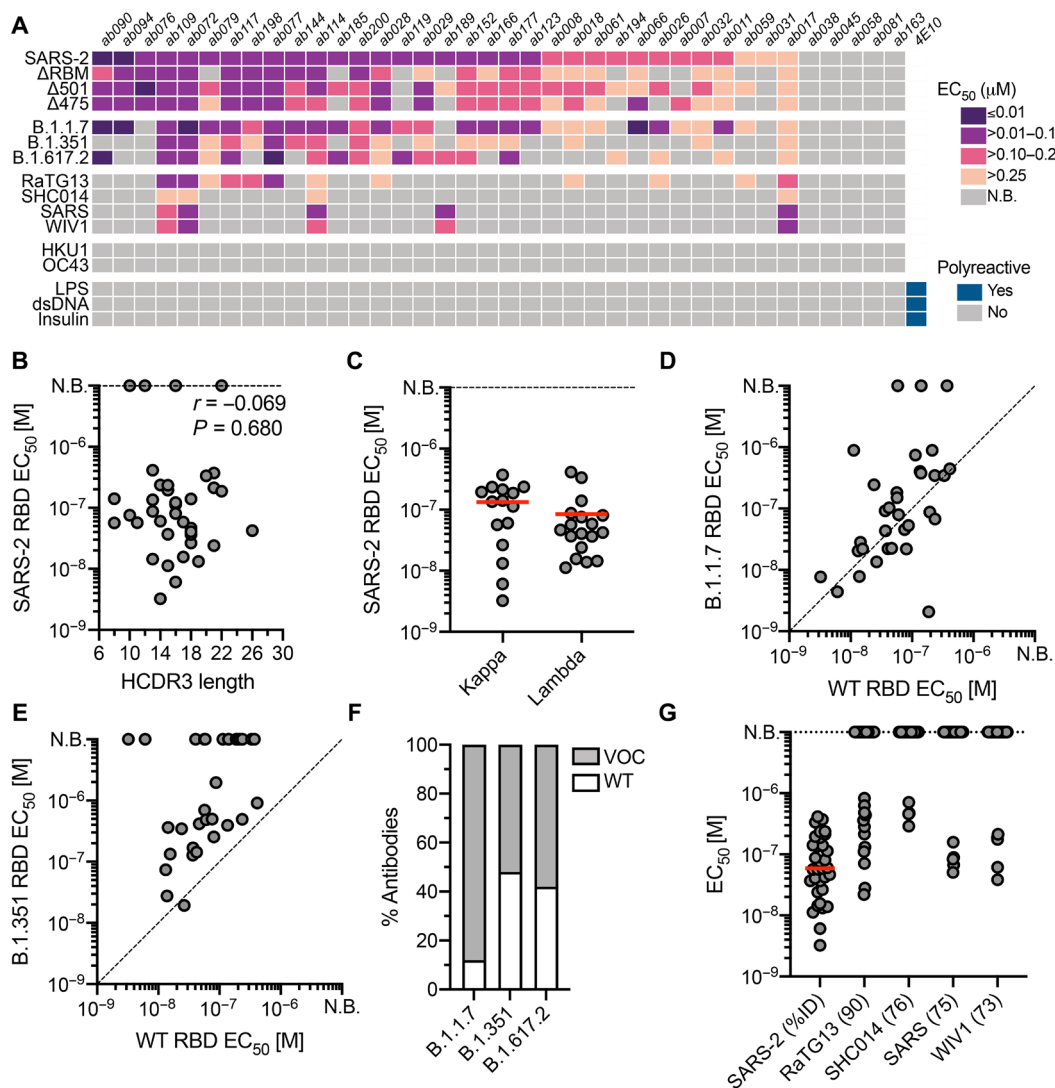

Fig. 2. Binding properties and specificity of isolated naive antibodies. (**A**) ELISA binding heat map of 38 naive IgGs. Binding to wild-type SARS-CoV-2 RBD (SARS-2), ΔRBM, individual RBD glycan variants, circulating variants, related CoVs, hCoVs, and polyreactive antigens. N.B., no binding. (**B**) Pearson correlation analysis of SARS-CoV-2 RBD affinities and HCDR3 length (IMGT) (*n* = 38). (**C**) ELISA EC_{50} values for IgGs with detectable SARS-CoV-2 RBD binding (*n* = 33) based on kappa or lambda gene usage. Red bars indicate the mean EC_{50} values. (**D**) Wild-type SARS-CoV-2 RBD ELISA EC_{50} values plotted against EC_{50} for B.1.1.7 RBD (**E**) and B.1.351 RBD. (**F**) Proportion of SARS-CoV-2 RBD binders with detectable ELISA affinity for variants of concern (VOC) B.1.1.7, B.1.351, and B.1.617.2 RBDs. (**G**) ELISA EC_{50} values to related sarbecovirus RBDs displayed in decreasing order of paired sequence identity.

reflected in the reduced ΔRBM median EC_{50} values (fig. S3E). We also identified examples of antibodies sensitive to only Δ475 (e.g., ab185) and only Δ501 (e.g., ab007) (Fig. 2A and fig. S3E).

To obtain binding kinetics independent of avidity effects from bivalent IgGs, 12 antibodies were selected for expression as antigen-binding fragments (Fabs) to determine monovalent binding affinity (K_Ds) by biolayer interferometry (BLI). Using monomeric RBD as the analyte, 10 of the 12 Fabs had detectable binding, with K_Ds ranging from ~6.5 to ~75 μM; the other two remaining Fabs (ab177 and ab185) gave unreliable affinity measurements (i.e., >100 μM) (fig. S4). All Fabs had characteristically fast off rates (k_{off}). This observation is consistent for germline B cells where fast off rates are compensated by avidity due to overall BCR surface density (25); subsequent affinity gains via SHM often result in slowing of the off rate and is a canonical mechanism of improved antigen binding (26).

Naive antibodies engage SARS-CoV-2 variants of concern

The emergence of SARS-CoV-2 variants with mutations in RBD has raised substantial concern that antigenic evolution will impair recognition of RBD-directed antibodies elicited by previous infection and vaccination with an antigenically distinct SARS-CoV-2 variant (27). We therefore asked whether these naive antibodies, isolated using wild-type SARS-CoV-2 RBD, could recognize circulating viral variants, B.1.1.7 (alpha; mutations N501Y), B.1.351 (beta; mutations K417N/E484K/N501Y), and B.1.617.2 (delta; L452R/T478K); the latter has become the most prevalent circulating variant in 2021. We find that ~89% of the antibodies with wild-type RBD affinity also bound to the B.1.1.7 variant with a comparable mean affinity of 68.7 nM (Fig. 2, D and F). For B.1.351, a concerning variant formerly prevalent in South Africa, 50% of the wild-type SARS-CoV-2 RBD-binding IgGs also bound to the B.1.351 variant, many of which displayed reduced ELISA binding relative to wild-type RBD with a mean affinity of 219 nM (Fig. 2, E and F). Last, ~58% of the antibodies with affinity for wild-type RBD also bound to the B.1.617.2 variant with a mean affinity of 100 nM (Fig. 2F and fig. S3A). A more pronounced reduction in cross-reactivity to the B.1.351 and B.1.617.2 variants may be predictive of reduced sera binding and neutralization titers from convalescent individuals and vaccine recipients (28).

Naive antibodies engage preemerging CoVs

We next tested the cross-reactivity of these naive antibodies to related sarbecovirus RBDs, which also use ACE2 as a host receptor (29). Our panel included the previously circulating SARS-CoV RBD and representative preemergent bat CoV RBDs from WIV1, RaTG13, and SHC014. These RBDs share ~73 to 90% paired sequence identity with the highest degree of amino acid conservation in residues outside of the RBM. Thirteen antibodies cross-reacted with at least one additional RBD in our panel, with decreasing affinity for RBDs with more divergent amino acid sequence identity (Fig. 2, A and G). ab017, ab072, ab109, and ab114 had broad reactivity to all tested sarbecovirus RBDs, suggesting binding to highly conserved epitopes. Of these cross-reactive antibodies, ab017 and ab114 derive from the same IGHV3-33 and IGVL2-14 pairing but were isolated from different donors, suggesting a shared or public clonotype.

Naive antibodies are not polyreactive and do not engage seasonal CoVs

Previous studies have shown that germline antibodies are more likely to display polyreactivity relative to affinity-matured antibodies with higher levels of SHM from mature B cell compartments (30). We therefore tested the polyreactivity of all 44 naive antibodies using three common autoantigens, double-stranded DNA (dsDNA), *Escherichia coli* lipopolysaccharide (LPS), and human insulin by ELISA (Fig. 2A) We observed no polyreactivity across any of the naive antibodies, including those that are broadly reactive. Furthermore, none of the naive antibodies bound RBDs from the human seasonal betacoronaviruses (hCoVs), OC43 and HKU1 (Fig. 2A), which share 22 and 19% paired sequence identity to SARS-CoV-2 RBD, respectively. Together, these results suggest that the isolated naive B cells encode BCRs with specificity to sarbecoviruses.

In vitro reconstitution of naive B cell activation

Physiological interactions between a naive BCR and cognate antigen occurs at the B cell surface. Naive BCRs are displayed as a bivalent membrane-bound IgM, and multivalent antigen binding can initiate intracellular signaling resulting in an activated B cell with the capacity to differentiate to antibody-secreting plasma cells or memory cells (1). To determine whether the isolated RBD-specific naive BCRs have the capacity to be activated, we generated stable Ramos B cell lines expressing ab090 or ab072 as cell surface BCRs and measured their activation by monitoring calcium flux in vitro (31). These antibodies were selected to represent divergent germline gene usage and specificities: (i) ab090 (IGHV1-2/IGKV3-15) bound SARS-CoV-2 and variant B.1.1.7 RBDs, but not variant B.1.351 and WIV1 RBDs (Fig. 3A), and (ii) ab072 (IGHV3-23/IGLV2-14) had broad reactivity to all RBDs (Fig. 3B). To assess BCR activation, we generated ferritin-based nanoparticles (NPs) for multivalent RBD display using SpyTag/SpyCatcher (32); these RBD NPs included SARS-CoV-2, B.1.1.7, B.1.351, and WIV RBDs. We found that ab090-expressing Ramos B cells were only activated by SARS-CoV-2 RBD and variant B.1.1.7 RBD NPs (Fig. 3C), whereas ab072 Ramos B cells were activated by all RBD NPs (Fig. 3D). These data parallel the observed recombinant binding specificity of each antibody. Neither ab090 nor ab072 Ramos B cell lines were activated by influenza hemagglutinin NPs, suggesting that this activation is sarbecovirus RBD specific (Fig. 3, C and D).

ab090 engages the SARS-CoV-2 RBM

To further characterize the epitope specificity of a representative naive antibody, we determined the structure of ab090 in complex with SARS-CoV-2 spike (S) by cryo–electron microscopy (cryo-EM). A ~6.7-Å structure showed one Fab bound to an RBD in the "up" conformation (Fig. 4, A and B, and fig. S5). On the basis of this modest resolution structure, we make the following general descriptions of the antibody-antigen interface. The interaction between ab090 and the RBD is mediated primarily by the antibody heavy chain, with the germline-encoded HCDR1, HCDR2, and the framework 3 DE loop centered over the RBM epitope (Fig. 4B). The ab090 light chain is oriented distal to the RBD and does not appear to substantially contribute to the paratope (Fig. 4B). IGHV1-2 antibodies represent a prevalent antibody class in human responses to SARS-CoV-2 infection, many of which display high neutralization potency (33). ab090 shares a V_H-centric mode of contact and angle of approach similar to members of this class of infection-elicited antibodies (Fig. 4D), despite varying HCDR3 lengths and diverse light chain pairings (Fig. 4D). In addition, members of the IGHV1-2 antibody class contain relatively few SHMs (fig. S5B). In conjunction with the structure, we biochemically defined the sensitivity of ab090 to variant B.1.351 by testing the binding to individual mutations.
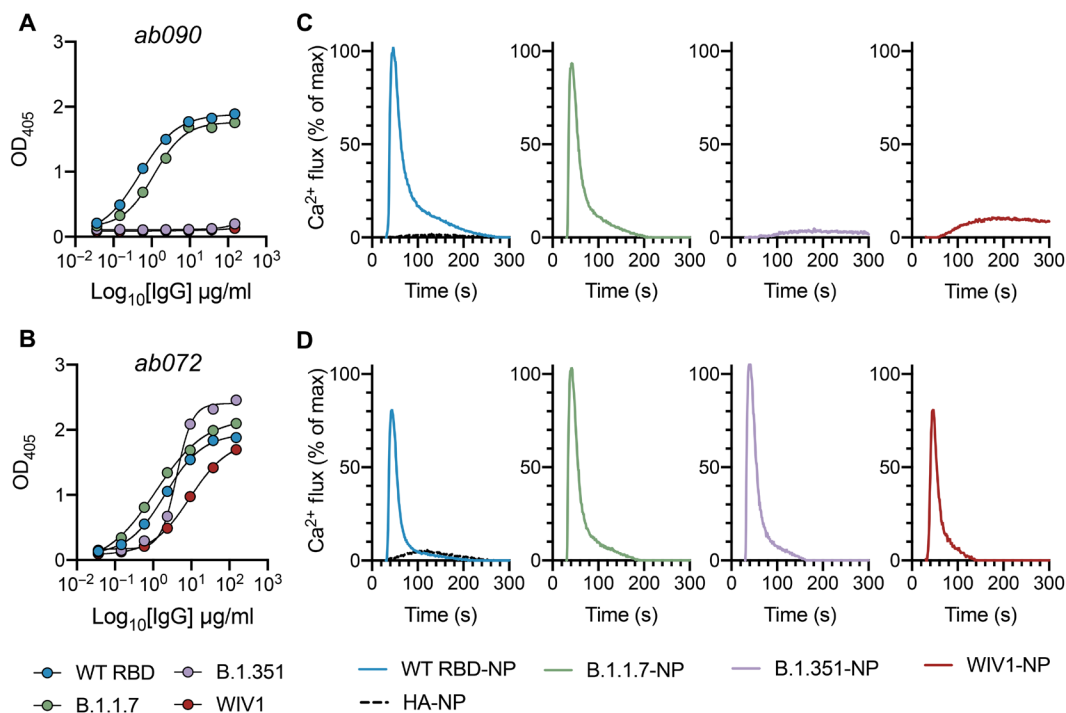
Fig. 3. In vitro reconstitution of naive B cell activation. (**A**) ELISA binding reactivity shows specificity of ab090 and ab072 (**B**) to wild-type (WT) SARS-CoV-2, B.1.1.7, B.1.351, and WIV1 RBDs. Data are presented as means ± SD of two technical replicates. (**C**) BCR activation as measured by calcium flux in a Ramos B cell line expressing ab090 membrane-anchored IgM (mIgM) and (**D**) ab072 mIgM in response to ferritin NPs displaying WT SARS-CoV-2, B.1.1.7, B.1.351, and WIV1 RBDs. Influenza hemagglutinin (HA) NP was used as a negative control. BCR cell line data are representative of two independent experiments.

Binding affinity was detected to SARS-CoV-2 RBDs with either N501Y or K417N mutations, but not to E484K alone (Fig. 4C). On the basis of the structure, the E484K mutation is grossly positioned proximal to the CDRH2 loop (Fig. 4C), which has a germline-encoded motif critical for IGHV1-2 antibody binding to RBD (fig. S5B) (33). Infection-elicited IGHV1-2 antibodies are susceptible to escape by E484K alone, which disrupts a CDRH2 hydrogen-binding network (34). Together, the cryo-EM structure and binding data suggest that ab090 represents a precursor of a class of RBM-directed SARS-CoV-2 neutralizing antibodies.

In vitro affinity-matured naive antibodies retain intrinsic specificity

After initial antigen recognition and subsequent activation, naive B cells can undergo successive rounds of SHM within the germinal center (GC) that ultimately result in higher-affinity antibodies for the cognate antigen. To determine how SHM might influence overall affinity and specificity, we used yeast surface display to in vitro mature ab072 and ab090. We randomly mutagenized the single-chain variable fragment (scFv) variable heavy and light chain regions to generate ab072 and ab090 variant display libraries. After two rounds of selection using SARS-CoV-2 RBD, we enriched the ab072 and ab090 libraries for improved binding over their respective parental clones (Fig. 5, A and D, and fig. S6A). We also observed increased binding to B.1.351 for the ab072 library but not for ab090; notably, this corresponded with the respective specificity of the parent clones (Fig. 5, A and D).

We next isolated and sequenced individual clones from the enriched libraries. For ab090, we observed a dominant mutation, R72H, in the FRWH3 region present in 60% of sequenced clones

(fig. S7B). Multiple mutations at position 72 conferred a nearly three- to fivefold improvement in monovalent affinity relative to parental ab090 for wild-type and B.1.1.7 RBDs, with no detectable B.1.351 binding for affinity-matured progeny (Fig. 5, B and C). In addition, ab090 progeny displayed a ~10-fold improvement in ELISA binding affinity (EC$_{50}$) to B.1.617.2 RBD (fig. S6E). We observed no mutations within the light chain, which is consistent with the V$_H$-centric binding mode in the cryo-EM structure (Fig. 4). For the broadly reactive ab072, isolated clones had mutations in both V$_H$ and V$_L$, and ~35% of the sequenced clones had mutation S31P in HCDR1 (fig. S7, B and C). There was 3- to ~5-fold improvement in monovalent affinity of ab072 progeny relative to parent for SARS-CoV-2, B.1.1.7, and B.1.351 RBDs (Fig. 5, E and F) and a ~14-fold improvement in binding to B.1.617.2 RBD by ELISA (fig. S6F). Collectively, these data identify potential mutations that can improve affinity while retaining initial parental antigen specificity.

SARS-CoV-2 pseudovirus neutralization by naive and affinity-matured antibodies

We next used a SARS-CoV-2 pseudovirus assay (6) to ask whether any of the isolated naive antibodies and affinity-matured clones were capable of blocking transduction of target cells. We found that, of the 36 RBD-binding antibodies tested in this assay, 5 had detectable levels of neutralization (~14%) (Fig. 6A). These antibodies, obtained from multiple donors, have no commonality with respect to their gene usages and HCDR3 lengths (Fig. 6B). Although these naive antibodies were not as potent as B38, isolated from a memory B cell, the observation that the naive repertoire has antibodies that neutralize is noteworthy nevertheless.
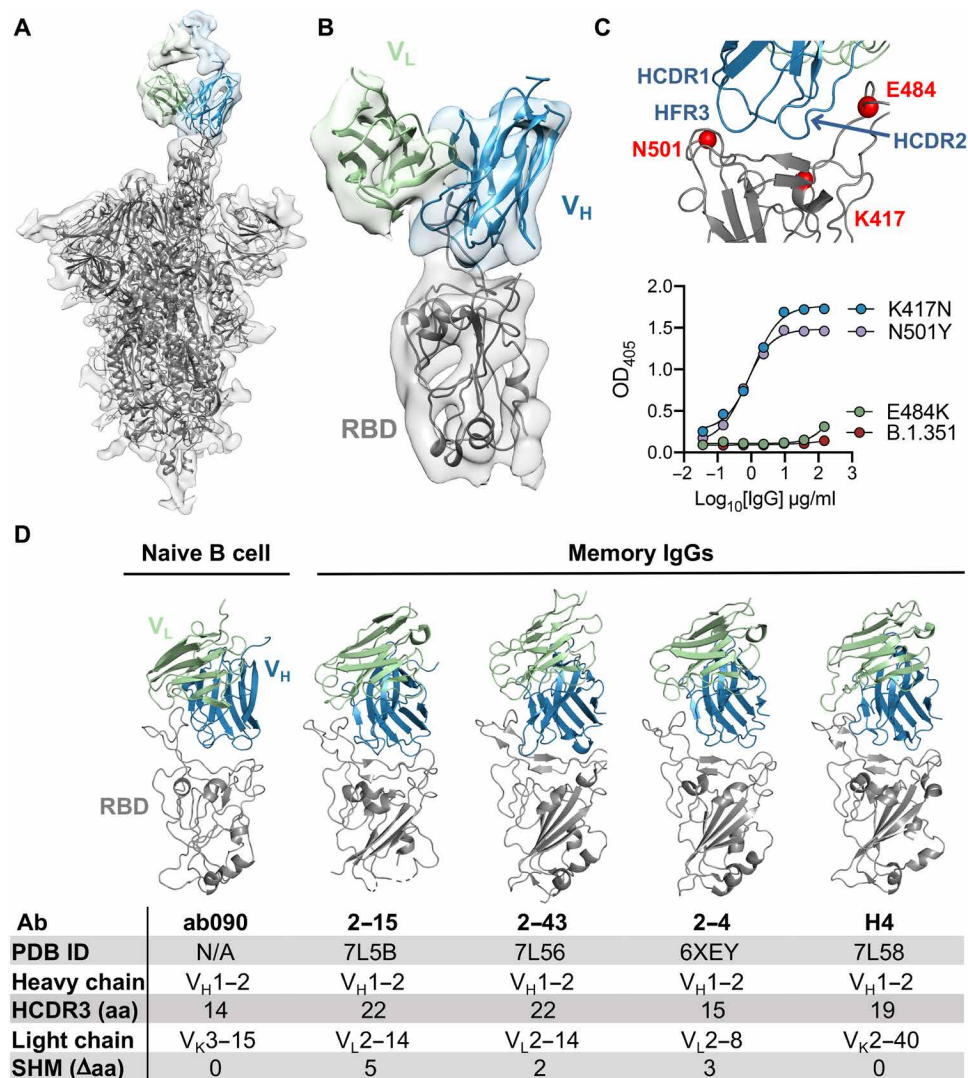
Fig. 4. ab090 recognizes the SARS-CoV-2 RBM. (**A**) Cryo-EM structure of the SARS-CoV-2 spike trimer (gray) with ab090 Fab bound to one RBD in the up position. (**B**) ab090 recognizes the SARS-CoV-2 RBM with a paratope centered on the V_H (blue). (**C**) Close-up view showing the approximate locations of HCDR loops proximal to the RBM epitope and B.1.351 RBD mutations highlighted in red (top). ELISA binding reactivity of ab090 to individual mutations from B.1.351 RBD (bottom). (**D**) ab090 and representative IGHV1-2 neutralizing antibodies (Ab) isolated from memory B cells from convalescent COVID-19 individuals bound to SARS-CoV-2 RBD (gray). Structures are shown in the same relative orientation in each panel, with PDB codes and sequence attributes listed in the below.

Ab	ab090	2–15	2–43	2–4	H4
	Naive B cell	**Memory IgGs**			
PDB ID	N/A	7L5B	7L56	6XEY	7L58
Heavy chain	V_H1–2	V_H1–2	V_H1–2	V_H1–2	V_H1–2
HCDR3 (aa)	14	22	22	15	19
Light chain	V_K3–15	V_L2–14	V_L2–14	V_L2–8	V_K2–40
SHM (Δaa)	0	5	2	3	0

To determine whether improved affinity correlated with enhanced neutralization potency, we evaluated the affinity-matured progeny of ab090 in a SARS-CoV-2 pseudovirus neutralization assay (Fig. 6B). We find that all three ab090 progeny that had higher affinity for SARS-CoV-2 RBD also had increased neutralization potency. ab090_A08 bearing the R72H mutation had the highest affinity gain and was the most potent neutralizer, with a K_D of 1.7 μM and a median inhibitory concentration (IC_{50}) of 0.37 μg/ml, respectively. ab090 progeny had IC_{50} values similar to other IGHV1-2 memory B cells isolated from convalescent donors (33); this increase in potency is conferred through minimal SHM.

DISCUSSION

The development of a protective humoral immune response upon infection or vaccination relies on the recruitment, activation, and maturation of antigen-specific naive B cells. However, the specificity of the naive B cell repertoire remains largely undefined. Here, we showed that CoV-specific naive B cells are present across distinct seronegative donors, are of unrestricted gene usage, and, when recombinantly expressed as IgGs, have affinity for SARS-CoV-2 RBD, circulating variants of concern, and at least four related CoVs. These data suggest that RBD-specific precursors are likely present across a large fraction of individual human naive repertories, consistent with longitudinal studies of SARS-CoV-2–infected individuals in which most convalescent individuals seroconverted with detectable RBD serum antibodies and neutralization titers (9, 35). The naive B cells characterized here engage epitopes across the RBD with a range of angles of approach as defined by our glycan variant probes and cross-reactivity profiles; this is also consistent with infection- and vaccine-elicited, RBD-specific repertoire characterized by epitope mapping, deep mutational scanning, and structural analyses (36, 37). Having naive BCRs recognizing distinct or partially overlapping epitopes across the RBD may be advantageous for eliciting a polyclonal response more able to recognize variants of concern.

The presence of broadly reactive naive B cells inherently capable of recognizing sarbecovirus RBDs and circulating variants suggests that these precursors could be vaccine-amplified. Recent work showed that uninfected individuals have preexisting SARS-CoV-2 S-reactive serum antibodies (38) and memory B cells (39), which cross-react with hCoVs and can be boosted upon SARS-CoV-2 infection. These cross-reactive antibodies appear to be specific to the S2 domain and are predominantly IgG or IgA. This observation contrasts the cross-reactive B cells described here that engage the RBD, have no reactivity to hCoVs, and are IgG⁻ naive B cells, suggesting that they are distinct from previously described S-reactive preexisting antibodies.

The competitive success of a naive B cell within a GC is influenced by precursor frequencies and antigen affinities (40). However, the biologically relevant affinities necessary for activation and GC entry remain unclear—several studies suggest that B cell activation and affinity maturation are not restricted by immeasurably low-affinity BCR interactions (41, 42). Recent studies involving naive precursors of receptor binding site (RBS)–directed HIV-1 broadly
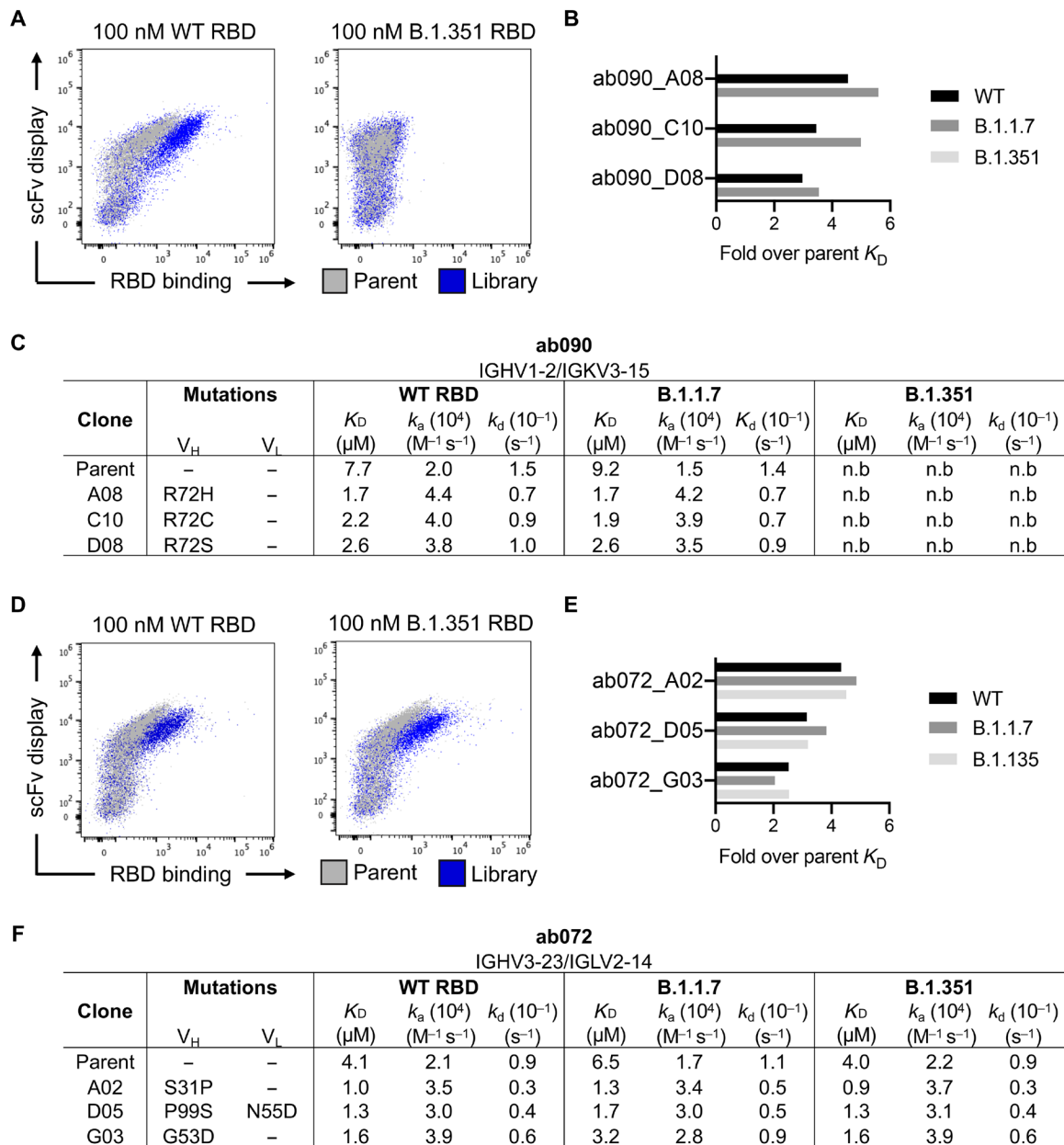
Fig. 5. In vitro affinity-matured naive antibodies retain intrinsic specificity. (**A**) Enrichment of ab090 parent (gray) and affinity-matured (blue) libraries to 100 nM SARS-CoV-2 or B.1.351 RBD using flow cytometry. (**B**) Fold enrichment in monovalent K_D over ab090 parent for selected affinity-matured progeny. (**C**) Kinetic analysis using BLI for ab090 parent and progeny Fabs to monomeric WT and variant RBDs. (**D**) Enrichment of ab072 parent (gray) and affinity-matured (blue) libraries to 100 nM SARS-CoV-2 or B.1.351 RBD using flow cytometry. (**E**) Fold enrichment in monovalent K_D over ab072 parent for selected affinity-matured progeny. (**F**) Kinetic analysis using BLI for ab072 parent and progeny Fabs to monomeric WT and variant RBDs. Kinetic data are calculated through global fit of titration curves from four independent antigen concentrations.

neutralizing antibodies contributed to our understanding of these parameters (*16*, *17*). Using an in vivo murine adoptive transfer model, these RBS-directed precursors were recruited into a GC reaction at a precursor frequency of ~1:10,000 and a monovalent antigen affinity of 14 µM (*17*). For comparison, here, we defined the SARS-CoV-2 RBM-specific naive precursor frequency as 1:42,000 by flow cytometric gating (fig. S2D), with monovalent affinities ranging from 6.5 to >100 µM. These data suggest that these isolated naive B cells, especially those with demonstrable monomeric affinity, could be

readily elicited upon antigen exposure. However, longitudinal studies tracking antigen-specific naive B cells before and after exposure are required to determine the fate (i.e., plasma cell, memory, or GC B cell compartments) of potential precursors and define relevant naive affinities for elicitation by SARS-CoV-2.

Precursor frequencies have recently been interrogated for human naive B cells targeting epitopes of broadly neutralizing HIV-1 and influenza antibodies, defined as 1:300,000 and 1:10,000, respectively (*15*, *43*). Although the frequency of SARS-CoV-2 RBM–specific
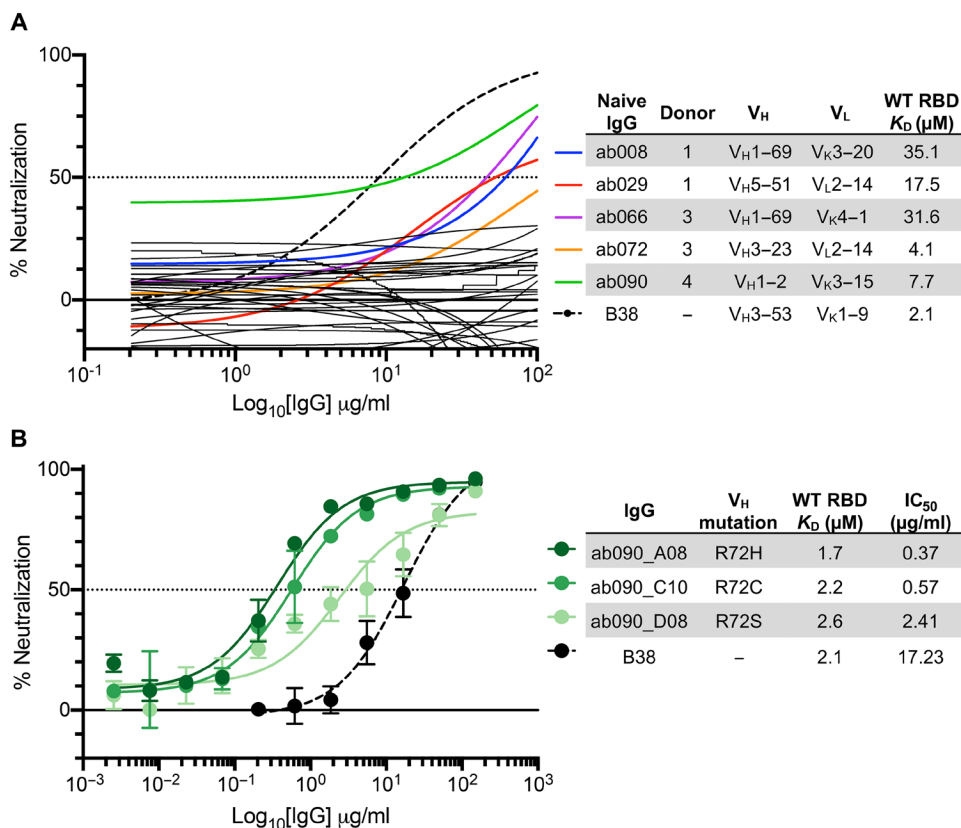
Fig. 6. SARS-CoV-2 pseudovirus neutralization by naive and affinity-matured antibodies. (**A**) SARS-CoV-2 pseudovirus neutralization assay for 32 purified IgGs. Curves in color highlighted antibodies with neutralizing activity with donor and monovalent wild-type RBD affinity listed for this subset of antibodies. The neutralizing monoclonal antibody, B38, was used as a positive control. Dashed lines indicate IC_{50} values, and data represent means ± SD of two technical replicates. (**B**) SARS-CoV-2 pseudovirus neutralization for select affinity-matured progeny from the ab090 lineage with respective mutations relative to ab090 parent sequence, monovalent wild-type RBD affinity, and IC_{50} listed.

naive precursors defined here (1:42,000) is within the range defined in these studies, we note that, in each case, precursor frequency will be unique for the antigen probe and will depend on the valency, affinity, and presentation of the target epitope. Furthermore, frequency alone does not account for SHM needed to attain neutralization potency.

Through biochemical and structural analyses, we characterized a naive antibody, ab090, which resembles a commonly elicited class of potent neutralizing antibodies using the IGHV1-2 gene (*33*). This class of antibodies shares restricted binding specificity for wild-type SARS-CoV RBD (the vaccine strain) and the prevalent B.1.1.7 variant. This recombinant binding pattern also paralleled the reconstituted in vitro B cell activation dynamics of ab090 in the highly avid assay with the capacity to detect immeasurably low affinity interactions (*25*). In vitro affinity maturation of ab090 corresponded to a single H-FR3 mutation, which improved monovalent affinity about fivefold to wild-type SARS-CoV-2 and B.1.1.7 RBDs relative to parent and pseudovirus neutralization to IC_{50} values less than 1 μg/ml. This observation is consistent with the low levels of SHM within IGHV1-2 neutralizing antibodies (*33*), with reports of other potent RBD-directed neutralizing antibodies with a limited level of SHM (*13*, *14*, *22*) and reports of neutralizing antibodies isolated in vitro from naive human antibody libraries (*44*). Although in vitro affinity

gains and neutralization potency are generally correlated (*45*), we note that affinity does not necessarily correlate to neutralization potency for all SARS-CoV-2 RBD targeting antibodies, where fine epitope specificity appears to be most relevant (*46*).

Probing and characterizing the human naive B cell antigen-specific repertoire can identify precursors for vaccine- or infection-specific naive B cells and expand our understanding of basic B cell biology. Germline-endowed specificity for neutralizing antibody targets on the RBD may also contribute to the strong clinical efficacy observed for the current SARS-CoV-2 vaccines (*47*, *48*). Furthermore, understanding the naive B cell repertoire to potential pandemic CoVs may reveal commonalties in antigen-specific precursors, enabling the development of pan-CoV vaccines aimed at engaging broadly protective germline responses.

MATERIALS AND METHODS
Study design
The aim of this study was to perform an in-depth analysis of the human naive B cell repertoire specific for a major target of SARS-CoV-2 neutralizing antibodies, the RBD of SARS-CoV-2. We isolated naive B cells from the peripheral blood of eight SARS-CoV-2 seronegative adults, sequenced the BCRs, and recombinantly expressed a diverse panel of IgGs from five of these donors for biochemical characterization. Sample sizes for each experiment are indicated in the figure legends.

Donor samples
Peripheral blood mononuclear cells (PBMCs) for single-cell sorting were isolated from eight blood donors from the Massachusetts General Hospital (MGH) Blood Donor Center. Before donation, individuals signed a donor consent statement, stating "I give permission for my blood to be used for transfusion to patients or for research." Patient samples were deidentified, but participants were a minimum of 16 years of age and weighed a minimum of 49.9 kg. All experiments were conducted with MGH Institutional Biosafety Committee approval (MGH protocol 2014B000035). Control human convalescent sera were obtained under the approved Partners Institutional Review Board (protocol 2020P000895) (*6*).

Expression and purification of recombinant CoV antigens
Plasmids encoding the RBDs were designed on the basis of GenBank sequences MN975262.1 (SARS-CoV-2), ABD72970.1 (SARS-CoV), AGZ48828.1 (WIV1), MN996532.2 (RaTG13), QJE50589.1 (SHC014), AAT98580.1 (HKU1), and AAT84362 (OC43). Constructs were codon-optimized and synthesized by Integrated DNA Technologies

(IDT). QuikChange Mutagenesis (Agilent) was used to insert glycosylation sites at SARS-CoV-2 RBD residues 501 and/or 475 and for RBD variants, B.1.351, B.1.1.7, and B.1.617.2. SARS-CoV-2 spike contained a C-terminal fold on trimerization domain and HRV 3C–cleavable 6xHis and 2xStrep II tags. Proteins were transiently expressed in Expi293F cells (Thermo Fisher Scientific). Five to 7 days after transfection, supernatants were harvested by centrifugation and purified using cobalt TALON resin (Takara) followed by size exclusion chromatography on a Superdex 200 Increase 10/300 GL column (GE Healthcare).

Expression and purification IgGs and Fabs
IgG and Fab genes for the heavy and light chain variable domains were synthesized, codon-optimized by IDT, subcloned into pVRC8400 protein expression vectors (49), and sequence-confirmed (Genewiz). Fabs and IgGs were similarly expressed and purified as described above for RBDs. IgGs were buffer-exchanged into phosphate-buffered saline (PBS), whereas Fabs were further purified by size exclusion chromatography (49).

Enzyme-linked immunosorbent assay
Sera and monoclonal antibody reactivity to CoV antigens were assayed by ELISA. Briefly, 96-well plates (Corning) were coated with monomeric RBDs (5 µg/ml) in PBS at 100 µl per well and incubated overnight at 4°C. Plates were blocked with 1% bovine serum albumin (BSA) in PBS containing 1% Tween 20 (PBS-T) for 1 hour at room temperature (RT). Blocking solution was discarded, and fourfold serial dilutions of human plasma (1:20 starting dilution) or isolated monoclonal antibodies (150 µg/ml starting concentration) in PBS were added to wells and incubated for 1 hour at RT. Plates were washed three times with PBS-T. Secondary, anti-human IgG–horseradish peroxidase (Abcam) was added at 1:20,000 dilution in PBS-T for 1 hour at RT. Plates were washed three times with PBS-T and developed with 1-Step ABTS substrate (Thermo Fisher Scientific). Absorbance was measured using a plate reader at 405 nm. EC_{50} values were determined by nonlinear regression (sigmoidal) using GraphPad Prism 8.4.3 software. ELISAs against OC43 and HKU1 RBDs were done at a single IgG concentration (150 µg/ml) in replicate. Positive binding was defined by OD_{405} (optical density at 405 nm) ≥ 0.30.

ELISAs for polyreactivity against human insulin (MilliporeSigma) and dsDNA (Calf Thymus DNA; Invitrogen) plates were coated with 2 and 50 µg/ml, respectively, in PBS and incubated overnight at 4°C. Plates were blocked and incubated with IgGs as described above. LPS ELISAs were measured as described (50). Briefly, plates were coated with LPS (30 µg/ml) (E. coli O55:B5; MilliporeSigma) in carbonate buffer for 3 hours at 37°C, washed three times with water, and air-dried overnight at RT. Coated plates were blocked with HS buffer [50 mM Hepes and 0.15 mM NaCl (pH 7.4)] plus BSA (10 mg/ml). Plates were incubated with IgGs diluted in HS buffer containing BSA (1 mg/ml) for 3 hours at 37°C, washed three times with HS buffer, and developed as described above. ELISAs that were performed at a single IgG concentration (15 µg/ml) in replicate with positive binding were defined by $OD_{405} \geq 0.30$.

ACE2 cell–binding assay
ACE2-expressing 293T cells were from M. Farzan (Scripps Florida) and N. Hacohen (Broad Institute) (6) and were incubated with 200 nM RBD antigen in PBS for 1 hour on ice. Cells were resuspended in 50 µl of secondary stain containing streptavidin-phycoerythrin

(PE) (Invitrogen) at a 1:200 dilution and incubated for 30 min on ice. Cell binding was analyzed by flow cytometry using a Stratedigm S1300Exi flow cytometer equipped with a 96-well plate high-throughput sampler. Resulting data were analyzed using FlowJo (10.7.1).

Probe generation
SARS-CoV-2 RBD and ΔRBM constructs were expressed as dimeric murine-Fc (mFc; IgG1) fusion proteins containing an HRV 3C–cleavable C-terminal 8xHis and streptavidin binding peptide (SBP) tags and purified as described above. SBP-tagged RBD- and ΔRBM-mFc dimers were mixed with fluorescently labeled streptavidin, SA-BV650 and SA-BV786 (BioLegend), to form RBD-mFc-BV650 and ΔRBM-mFc-BV786 tetramers. SARS-CoV-2 spike with a C-terminal Strep II tag was labeled separately with Strep-Tactin PE and allophycocyanin (APC) (IBA) to form spike-PE and spike-APC tetramers, respectively. Both labeling steps were performed for 30 min at 4°C before sorting.

Single B cell sorting
Naive B cells were purified from PBMCs using the MACS Human B Cell Isolation Kit (Miltenyi Biotec) and incubated with 25 nM of each SARS-CoV-2 probe (RBD-mFc-BV650, ΔRBM-mFc-BV786, spike-PE, and spike-APC) for 30 min at 4°C. Cells were stained with anti-human CD19 (Alexa Fluor 700; BioLegend, catalog no. 302226), CD3 (PerCP-Cy5; BD Biosciences, catalog no. 560835), IgD (PE-Cy7; BD Biosciences, catalog no. 561314), IgG (BV711; BD Biosciences, catalog no. 740796), CD27 (BV510; BD Biosciences, catalog no. 750167), LIVE/DEAD violet (Invitrogen), and calcein (Invitrogen) for an additional 30 min. RBM-specific naive B cells, defined as CD19+/CD3−/IgG−/IgD+/spike PE+/spike APC+/RBD+/ΔRBM−, were single-cell–sorted using BD FACSAria II (BD Biosciences) into 96-well plates containing lysis buffer supplemented with 1% 2-mercaptoethanol (BME). Within the CD19+/IgG−/IgD+ gated cells, we also confirmed that 97% of the events were CD27 negative. Plates were stored at −80°C for subsequent analysis. Flow cytometry data were analyzed using FlowJo software version 10.7.1.

BCR sequencing
BCR sequencing was carried out as described previously (15). Briefly, whole-transcriptome amplification was performed on the sorted cell lysates according to the Smart-Seq2 protocol (51). Heavy and light chain sequences were amplified using partially degenerate pools of V region–specific primers (QIAGEN HotStarTaq Plus). Heavy and light chain amplifications were carried out separately. Cellular barcodes and index adapters (based on Nextera XT Index Adapters, Illumina Inc.) were added using a step-out polymerase chain reaction (PCR) method. Amplicons were pooled and sequenced using a 250 × 250 paired end 8 × 8 index reads on an Illumina MiSeq system. Data were demultiplexed, heavy and light chain reads were paired, and overlapping sequence reads were obtained (PANDAseq) (52) and aligned against the human international ImMunoGeneTics information system (IMGT) database.

Interferometry binding experiments
Interferometry experiments were performed using a BLItz instrument (ForteBio). Fabs (0.1 mg/ml) were immobilized on Ni–nitrilotriacetic acid biosensors. The SARS-CoV-2 RBD analyte was titrated (10, 5, 2.5, and 1 µM) to acquire binding affinities; K_D was obtained through global fit of the titration curves by applying a 1:1 binding isotherm using vendor-supplied software.

Pseudotyped neutralization assay

SARS-CoV-2 neutralization was assessed using lentiviral particles pseudotyped as previously described (6). Briefly, lentiviral particles were produced via transient transfection of 293T cells. The titers of viral supernatants were determined via flow cytometry on 293T-ACE2 cells and via the HIV-1 p24^{CA} antigen capture assay (Leidos Biomedical Research Inc.). Assays were performed in 384-well plates (Grenier) using a Fluent Automated Workstation (Tecan). IgGs, starting at 150 µg/ml, were serially diluted (threefold) in 20 µl followed by addition of 20 µl of pseudovirus containing 250 infectious units and incubated at RT for 1 hour. Last, 10,000 293T-ACE2 cells in 20 µl of cell medium containing polybrene (15 µg/ml) were added to each well and incubated at 37°C for 60 to 72 hours. After transduction, cells were lysed and shaken for 5 min before quantitation of luciferase expression using a SpectraMax L luminometer (Molecular Devices). Percent neutralization was determined by subtracting background luminescence measured from cell control wells (cells only) from sample wells and dividing by virus control wells (virus and cells only). Data were analyzed using GraphPad Prism.

Cryo-EM sample preparation, data collection, and processing

SARS-CoV-2 spike HexaPro was incubated with ab090 Fab at 0.6 mg/ml at a molar ratio of 1.5:1 Fab:spike for 20 min at 4°C, and two 3-µl aliquots were applied to UltrAuFoil gold R0.6/1 grids, subsequently blotted for 3 s at blot force 3 twice, and then plunge-frozen in liquid ethane using FEI Vitrobot Mark IV. Grids were imaged on a Titan Krios microscope operated at 300 kV and equipped with a Gatan K3 Summit direct detector. A total of 10,690 movies were collected in counting mode at 16e^-/pixel per second at a magnification of 81,000, corresponding to a calibrated pixel size of 1.058 Å. Defocus values were at around −2.00 µm. Micrographs were aligned and dose-weighted using RELION's (53) implementation of MotionCorr2 (54). Contrast transfer function estimation was done in GCTF (55). Particles were picked with crYOLO (56) with a model trained with 12 manually picked micrographs with a particle diameter value of 330 Å. Initial processing was performed in RELION. Particles were binned to ~12 Å/pixel and two-dimensionally (2D) classified. Selected particles were extracted to ~6 Å/pixel and then subjected to a second round of 2D classification. An initial model was generated at ~6 Å/pixel and used as a reference for two rounds of 3D classification: first to select particles containing SARS-CoV-2 spike and then to select particles containing both spike and ab090. Selected particles were unbinned and then aligned using 3D auto-refine and subjected to a third round of 3D classification to select for a single class with SARS-CoV-2 spike bound with one ab090 Fab. Selected particles were aligned using 3D auto-refine before undergoing CTF refinement and Bayesian polishing. Polished particles were then simultaneously focus-aligned relative to the RBD and ab090 region (fig. S5A) to aid in model building of this region of interest and imported to cryoSPARC (57). Imported particles were aligned using nonuniform refinement and local resolution estimation (fig. S5B). Nonuniform refined maps were then sharpened with DeepEMhancer and then used to dock a previously built SARS-CoV-2 spike model [Protein Data Bank identification (PDB) ID 7LQW].

Cryo-EM model building

Backbone models were built by docking variable regions from PDB ID 2D2P and 6FG1 for heavy and light chains, respectively, and an RBD (PDB 6M0J) into the focus-refined maps using UCSF Chimera (58) variable regions was corrected and manually built using COOT (59). For the remainder of the spike, a previously published model (PDB ID 6VXX) was docked into the full sharpened map in UCSF Chimera.

RBD NP production and conjugation

Monomeric SARS-CoV-2 wild-type, B.1.1.7, B.1.351, and WIV1 RBDs were recombinantly produced and purified as described above with an 8xHis and SpyTag at the C terminus. *Helicobacter pylori* ferritin NPs were expressed separately with N-terminal 8xHis and SpyCatcher tags. SpyTag-SpyCatcher conjugations were performed overnight at 4°C, with a fourfold molar excess of SpyTag-RBD relative to SpyCatcher-NP. The conjugated RBD NPs were repurified by size exclusion chromatography to remove excess RBD SpyTag.

In vitro BCR stimulation

Briefly, BCRs for ab090 and ab072 were stably expressed in an IgM-negative Ramos B cell clone by lentiviral transduction (31). Five to 7 days after transduction, BCR-expressing B cells were fluorescence-activated cell sorting (FACS)–sorted on IgM (APC anti-human IgM; BioLegend, catalog no. 314510) and kappa light chain (PE anti-human kappa light chain; eBioscience, catalog no. 12-9970-42) double positivity using the SH800S Cell Sorter (Sony Biotechnology). Sorted cells were expanded in RPMI 1640 and evaluated for B cell activation by labeling 10 million cells with Fura Red dye (0.5 µg/ml) (Invitrogen) in 2 ml of RPMI 1640 at 37°C for 30 min. Cells were washed and resuspended to 4 million cells/ml in RPMI 1640. BCR triggering was measured in response to the RBD NPs described above by flow cytometry (BD LSR II, BD Biosciences) as the ratio of Ca^{2+} bound/unbound states of Fura Red. Ratiometric measures for individual B cell lines were normalized to the maximum Ca^{2+} flux as measured by exposure to ionomycin (10 µg/ml).

In vitro affinity maturation of ab090 and ab072

Mutagenized yeast displays libraries for ab090 and ab072 scFvs by error-prone PCR using the GeneMorph II Random Mutagenesis Kit (Agilent Technologies). Mutagenized scFv DNA products were combined with the linearized yeast display vector pCHA (60) and electroporated into EBY100 grown to mid-log phase in YPD (yeast extract, peptone, and dextrose) medium, where the full plasmid was reassembled by homologous recombination. The final library size was estimated to be ~4 × 10^7. The scFv libraries were passaged in selective synthetic dextrose casamino acid (SDCAA) medium at 30°C and induced with galactose at 20°C (60). The scFv libraries were induced 10-fold over their respective diversities and subjected to three rounds of selection with SBP-tagged SARS-CoV-2 RBD-Fc. Induced yeast libraries were stained for antigen binding (RBD-Fc APC tetramers) and scFv expression (chicken anti–c-myc IgY; Invitrogen, catalog no. A-21281). After two washes in PBS with 0.1% (w/v) BSA, yeast was stained with donkey anti-chicken IgY AF488 (Jackson ImmunoResearch, catalog no. 703-545-155). Two gates were drawn for cells with improved RBD binding over parental clones: A more stringent "edge" gate represented ~1% of the improved output, and a "diversity" gate represented ~3 to 5% of the improved output. Clones from the final round of selection were isolated and Sanger-sequenced for recombinant IgG and Fab expression.

SUPPLEMENTARY MATERIALS

www.science.org/doi/10.1126/sciimmunol.abl5842
Figs. S1 to S6
Table S1
Data file S1

View/request a protocol for this paper from *Bio-protocol*.

REFERENCES AND NOTES

1. N. E. Harwood, F. D. Batista, Early events in B cell activation. *Annu. Rev. Immunol.* **28**, 185–210 (2010).
2. G. D. Victora, M. C. Nussenzweig, Germinal centers. *Annu. Rev. Immunol.* **30**, 429–457 (2012).
3. F. Sallusto, A. Lanzavecchia, K. Araki, R. Ahmed, From vaccines to memory and back. *Immunity* **33**, 451–463 (2010).
4. W. Deng, L. Bao, J. Liu, C. Xiao, J. Liu, J. Xue, Q. Lv, H. Gao, P. Yu, Y. Xu, Y. Qu, F. Li, Z. Xiang, H. Yu, S. Gong, M. Liu, G. Wang, S. Wang, Z. Song, Y. Liu, W. Zhao, Y. Han, L. Zhao, X. Liu, Q. Wei, C. Qin, Primary exposure to SARS-CoV-2 protects against reinfection in rhesus macaques. *Science* **369**, 818–823 (2020).
5. N. B. Mercado, R. Zahn, F. Wegmann, C. Loos, A. Chandrashekar, J. Yu, J. Liu, L. Peter, K. McMahan, L. H. Tostanoski, X. He, D. R. Martinez, L. Rutten, R. Bos, D. van Manen, J. Vellinga, J. Custers, J. P. Langedijk, T. Kwaks, M. J. G. Bakkers, D. Zuijdgeest, S. K. R. Huber, C. Atyeo, S. Fischinger, J. S. Burke, J. Feldman, B. M. Hauser, T. M. Caradonna, E. A. Bondzie, G. Dagotto, M. S. Gebre, E. Hoffman, C. Jacob-Dolan, M. Kirilova, Z. Li, Z. Lin, S. H. Mahrokhian, L. F. Maxfield, F. Nampanya, R. Nityanandam, J. P. Nkolola, S. Patel, J. D. Ventura, K. Verrington, H. Wan, L. Pessaint, A. Van Ry, K. Blade, A. Strasbaugh, M. Cabus, R. Brown, A. Cook, S. Zouantchangadou, E. Teow, H. Andersen, M. G. Lewis, Y. Cai, B. Chen, A. G. Schmidt, R. K. Reeves, R. S. Baric, D. A. Lauffenburger, G. Alter, P. Stoffels, M. Mammen, J. Van Hoof, H. Schuitemaker, D. H. Barouch, Single-shot Ad26 vaccine protects against SARS-CoV-2 in rhesus macaques. *Nature* **586**, 583–588 (2020).
6. W. F. Garcia-Beltran, E. C. Lam, M. G. Astudillo, D. Yang, T. E. Miller, J. Feldman, B. M. Hauser, T. M. Caradonna, K. L. Clayton, A. D. Nitido, M. R. Murali, G. Alter, R. C. Charles, A. Dighe, J. A. Branda, J. K. Lennerz, D. Lingwood, A. G. Schmidt, A. J. Iafrate, A. B. Balazs, COVID-19-neutralizing antibodies predict disease severity and survival. *Cell* **184**, 476–488.e11 (2021).
7. D. S. Khoury, D. Cromer, A. Reynaldi, T. E. Schlub, A. K. Wheatley, J. A. Juno, K. Subbarao, S. J. Kent, J. A. Triccas, M. P. Davenport, Neutralizing antibody levels are highly predictive of immune protection from symptomatic SARS-CoV-2 infection. *Nat. Med.* **27**, 1205–1211 (2021).
8. J. S. Turner, W. Kim, E. Kalaidina, C. W. Goss, A. M. Rauseo, A. J. Schmitz, L. Hansen, A. Haile, M. K. Klebert, I. Pusic, J. A. O'Halloran, R. M. Presti, A. H. Ellebedy, SARS-CoV-2 infection induces long-lived bone marrow plasma cells in humans. *Nature* **595**, 421–425 (2021).
9. J. M. Dan, J. Mateus, Y. Kato, K. M. Hastie, E. D. Yu, C. E. Faliti, A. Grifoni, S. I. Ramirez, S. Haupt, A. Frazier, C. Nakao, V. Rayaprolu, S. A. Rawlings, B. Peters, F. Krammer, V. Simon, E. O. Saphire, D. M. Smith, D. Weiskopf, A. Sette, S. Crotty, Immunological memory to SARS-CoV-2 assessed for up to 8 months after infection. *Science* **371**, eabf4063 (2021).
10. G. E. Hartley, E. S. J. Edwards, P. M. Aui, N. Varese, S. Stojanovic, J. McMahon, A. Y. Peleg, I. Boo, H. E. Drummer, P. M. Hogarth, R. E. O'Hehir, M. C. van Zelm, Rapid generation of durable B cell memory to SARS-CoV-2 spike and nucleocapsid proteins in COVID-19 and convalescence. *Sci. Immunol.* **5**, eabf8891 (2020).
11. Z. Wang, F. Schmidt, Y. Weisblum, F. Muecksch, C. O. Barnes, S. Finkin, D. Schaefer-Babajew, M. Cipolla, C. Gaebler, J. A. Lieberman, T. Y. Oliveira, Z. Yang, M. E. Abernathy, K. E. Huey-Tubman, A. Hurley, M. Turroja, K. A. West, K. Gordon, K. G. Millard, V. Ramos, J. D. Silva, J. Xu, R. A. Colbert, R. Patel, J. Dizon, C. Unson-O'Brien, I. Shimeliovich, A. Gazumyan, M. Caskey, P. J. Bjorkman, R. Casellas, T. Hatziioannou, P. D. Bieniasz, M. C. Nussenzweig, mRNA vaccine-elicited antibodies to SARS-CoV-2 and circulating variants. *Nature* **592**, 616–622 (2021).
12. C. O. Barnes, C. A. Jette, M. E. Abernathy, K.-M. A. Dam, S. R. Esswein, H. B. Gristick, A. G. Malyutin, N. G. Sharaf, K. E. Huey-Tubman, Y. E. Lee, D. F. Robbiani, M. C. Nussenzweig, A. P. West Jr., P. J. Bjorkman, SARS-CoV-2 neutralizing antibody structures inform therapeutic strategies. *Nature* **588**, 682–687 (2020).
13. C. Kreer, M. Zehner, T. Weber, M. S. Ercanoglu, L. Gieselmann, C. Rohde, S. Halwe, M. Korenkov, P. Schommers, K. Vanshylla, V. D. Cristanziano, H. Janicki, R. Brinker, A. Ashurov, V. Krähling, A. Kupke, H. Cohen-Dvashi, M. Koch, J. M. Eckert, S. Lederer, N. Pfeifer, T. Wolf, M. J. G. T. Vehreschild, C. Wendtner, R. Diskin, H. Gruell, S. Becker, F. Klein, Longitudinal isolation of potent near-germline SARS-CoV-2-neutralizing antibodies from COVID-19 patients. *Cell* **182**, 843–854.e12 (2020).
14. S. J. Zost, P. Gilchuk, R. E. Chen, J. B. Case, J. X. Reidy, A. Trivette, R. S. Nargi, R. E. Sutton, N. Suryadevara, E. C. Chen, E. Binshtein, S. Shrihari, M. Ostrowski, H. Y. Chu, J. E. Didier, K. W. MacRenaris, T. Jones, S. Day, L. Myers, F. E.-H. Lee, D. C. Nguyen, I. Sanz, D. R. Martinez, P. W. Rothlauf, L.-M. Bloyet, S. P. J. Whelan, R. S. Baric, L. B. Thackray, M. S. Diamond, R. H. Carnahan, J. E. Crowe Jr., Rapid isolation and profiling of a diverse panel of human monoclonal antibodies targeting the SARS-CoV-2 spike protein. *Nat. Med.* **26**, 1422–1427 (2020).
15. M. Sangesland, L. Ronsard, S. W. Kazer, J. Bals, S. Boyoglu-Barnum, A. S. Yousif, R. Barnes, J. Feldman, M. Quirindongo-Crespo, P. M. McTamney, D. Rohrer, N. Lonberg, B. Chackerian, B. S. Graham, M. Kanekiyo, A. K. Shalek, D. Lingwood, Germline-encoded affinity for cognate antigen enables vaccine amplification of a human broadly neutralizing response against influenza virus. *Immunity* **51**, 735–749.e8 (2019).
16. P. Dosenovic, E. E. Kara, A.-K. Pettersson, A. T. McGuire, M. Gray, H. Hartweger, E. S. Thientosapol, L. Stamatatos, M. C. Nussenzweig, Anti-HIV-1 B cell responses are dependent on B cell precursor frequency and antigen-binding affinity. *Proc. Natl. Acad. Sci. U.S.A.* **115**, 4743–4748 (2018).
17. R. K. Abbott, J. H. Lee, S. Menis, P. Skog, M. Rossi, T. Ota, D. W. Kulp, D. Bhullar, O. Kalyuzhniy, C. Havenar-Daughton, W. R. Schief, D. Nemazee, S. Crotty, Precursor frequency and affinity determine B cell competitive fitness in germinal centers, tested with germline-targeting HIV vaccine immunogens. *Immunity* **48**, 133–146.e6 (2018).
18. J. G. Jardine, D. W. Kulp, C. Havenar-Daughton, A. Sarkar, B. Briney, D. Sok, F. Sesterhenn, J. Ereño-Orbea, O. Kalyuzhniy, I. Deresa, X. Hu, S. Spencer, M. Jones, E. Georgeson, Y. Adachi, M. Kubitz, A. C. deCamp, J.-P. Julien, I. A. Wilson, D. R. Burton, S. Crotty, W. R. Schief, HIV-1 broadly neutralizing antibody precursor B cells revealed by germline-targeting immunogen. *Science* **351**, 1458–1463 (2016).
19. B. M. Hauser, M. Sangesland, E. C. Lam, J. Feldman, A. S. Yousif, T. M. Caradonna, A. B. Balazs, D. Lingwood, A. G. Schmidt, Engineered receptor binding domain immunogens elicit pan-coronavirus neutralizing antibodies. bioRxiv 2020.12.07.415216 [**Preprint**]. 8 December 2020. https://doi.org/10.1101/2020.12.07.415216.
20. B. Briney, A. Inderbitzin, C. Joyce, D. R. Burton, Commonality despite exceptional diversity in the baseline human antibody repertoire. *Nature* **566**, 393–397 (2019).
21. B. Ju, Q. Zhang, J. Ge, R. Wang, J. Sun, X. Ge, J. Yu, S. Shan, B. Zhou, S. Song, X. Tang, J. Yu, J. Lan, J. Yuan, H. Wang, J. Zhao, S. Zhang, Y. Wang, X. Shi, L. Liu, J. Zhao, X. Wang, Z. Zhang, L. Zhang, Human neutralizing antibodies elicited by SARS-CoV-2 infection. *Nature* **584**, 115–119 (2020).
22. S. C. A. Nielsen, F. Yang, K. J. L. Jackson, R. A. Hoh, K. Röltgen, G. H. Jean, B. A. Stevens, J.-Y. Lee, A. Rustagi, A. J. Rogers, A. E. Powell, M. Hunter, J. Najeeb, A. R. Otrelo-Cardoso, K. E. Yost, B. Daniel, K. C. Nadeau, H. Y. Chang, A. T. Satpathy, T. S. Jardetzky, P. S. Kim, T. T. Wang, B. A. Pinsky, C. A. Blish, S. D. Boyd, Human B cell clonal expansion and convergent antibody responses to SARS-CoV-2. *Cell Host Microbe* **28**, 516–525.e5 (2020).
23. I. C. MacLennan, K. M. Toellner, A. F. Cunningham, K. Serre, D. M. Y. Sze, E. Zúñiga, M. C. Cook, C. G. Vinuesa, Extrafollicular antibody responses. *Immunol. Rev.* **194**, 8–18 (2003).
24. D. F. Robbiani, C. Gaebler, F. Muecksch, J. C. C. Lorenzi, Z. Wang, A. Cho, M. Agudelo, C. O. Barnes, A. Gazumyan, S. Finkin, T. Hägglöf, T. Y. Oliveira, C. Viant, A. Hurley, H.-H. Hoffmann, K. G. Millard, R. G. Kost, M. Cipolla, K. Gordon, F. Bianchini, S. T. Chen, V. Ramos, R. Patel, J. Dizon, I. Shimeliovich, P. Mendoza, H. Hartweger, L. Nogueira, M. Pack, J. Horowitz, F. Schmidt, Y. Weisblum, E. Michailidis, A. W. Ashbrook, E. Waltari, J. E. Pak, K. E. Huey-Tubman, N. Koranda, P. R. Hoffman, A. P. West, C. M. Rice, T. Hatziioannou, P. J. Bjorkman, P. D. Bieniasz, M. Caskey, M. C. Nussenzweig, Convergent antibody responses to SARS-CoV-2 in convalescent individuals. *Nature* **584**, 437–442 (2020).
25. D. Lingwood, P. M. McTamney, H. M. Yassine, J. R. Whittle, X. Guo, J. C. Boyington, C.-J. Wei, G. J. Nabel, Structural and genetic basis for development of broadly neutralizing influenza antibodies. *Nature* **489**, 566–570 (2012).
26. F. D. Batista, M. S. Neuberger, Affinity dependence of the B cell response to antigen: A threshold, a ceiling, and the importance of off-rate. *Immunity* **8**, 751–759 (1998).
27. P. Wang, M. S. Nair, L. Liu, S. Iketani, Y. Luo, Y. Guo, M. Wang, J. Yu, B. Zhang, P. D. Kwong, B. S. Graham, J. R. Mascola, J. Y. Chang, M. T. Yin, M. Sobieszczyk, C. A. Kyratsous, L. Shapiro, Z. Sheng, Y. Huang, D. D. Ho, Antibody resistance of SARS-CoV-2 variants B.1.351 and B.1.1.7. *Nature* **593**, 130–135 (2021).
28. W. F. Garcia-Beltran, E. C. Lam, K. S. Denis, A. D. Nitido, Z. H. Garcia, B. M. Hauser, J. Feldman, M. N. Pavlovic, D. J. Gregory, M. C. Poznansky, A. Sigal, A. G. Schmidt, A. J. Iafrate, V. Naranbhai, A. B. Balazs, Multiple SARS-CoV-2 variants escape neutralization by vaccine-induced humoral immunity. *Cell* **184**, 2372–2383.e9 (2021).
29. M. Letko, A. Marzi, V. Munster, Functional assessment of cell entry and receptor usage for SARS-CoV-2 and other lineage B betacoronaviruses. *Nat. Microbiol.* **5**, 562–569 (2020).
30. L. Shehata, D. P. Maurer, A. Z. Wec, A. Lilov, E. Champney, T. Sun, K. Archambault, I. Burnina, H. Lynaugh, X. Zhi, Y. Xu, L. M. Walker, Affinity maturation enhances antibody specificity but compromises conformational stability. *Cell Rep.* **28**, 3300–3308.e4 (2019).
31. G. C. Weaver, R. F. Villar, M. Kanekiyo, G. J. Nabel, J. R. Mascola, D. Lingwood, In vitro reconstitution of B cell receptor–antigen interactions to evaluate potential vaccine candidates. *Nat. Protoc.* **11**, 193–213 (2016).
32. A. A. Cohen, P. N. P. Gnanapragasam, Y. E. Lee, P. R. Hoffman, S. Ou, L. M. Kakutani, J. R. Keeffe, H.-J. Wu, M. Howarth, A. P. West, C. O. Barnes, M. C. Nussenzweig, P. J. Bjorkman, Mosaic nanoparticles elicit cross-reactive immune responses to zoonotic coronaviruses in mice. *Science* **371**, 735–741 (2021).
33. M. Rapp, Y. Guo, E. R. Reddem, J. Yu, L. Liu, P. Wang, G. Cerutti, P. Katsamba, J. S. Bimela, F. A. Bahna, S. M. Mannepalli, B. Zhang, P. D. Kwong, Y. Huang, D. D. Ho, L. Shapiro,

Z. Sheng, Modular basis for potent SARS-CoV-2 neutralization by a prevalent VH1-2–derived antibody class. *Cell Rep.* **35**, 108950 (2021).

34. M. Yuan, D. Huang, C.-C. D. Lee, N. C. Wu, A. M. Jackson, X. Zhu, H. Liu, L. Peng, M. J. van Gils, R. W. Sanders, D. R. Burton, S. M. Reincke, H. Prüss, J. Kreye, D. Nemazee, A. B. Ward, I. A. Wilson, Structural and functional ramifications of antigenic drift in recent SARS-CoV-2 variants. *Science*, eabh1139 (2021).

35. K. Vanshylla, V. Di Cristanziano, F. Kleipass, F. Dewald, P. Schommers, L. Gieselmann, H. Gruell, M. Schlotz, M. S. Ercanoglu, R. Stumpf, P. Mayer, M. Zehner, E. Heger, W. Johannis, C. Horn, I. Suárez, N. Jung, S. Salomon, K. A. Eberhardt, B. Gathof, G. Fätkenheuer, N. Pfeifer, R. Eggeling, M. Augustin, C. Lehmann, F. Klein, Kinetics and correlates of the neutralizing antibody response to SARS-CoV-2 infection in humans. *Cell Host Microbe* **29**, 917–929.e4 (2021).

36. L. Piccoli, Y.-J. Park, M. A. Tortorici, N. Czudnochowski, A. C. Walls, M. Beltramello, C. Silacci-Fregni, D. Pinto, L. E. Rosen, J. E. Bowen, O. J. Acton, S. Jaconi, B. Guarino, A. Minola, F. Zatta, N. Sprugasci, J. Bassi, A. Peter, A. De Marco, J. C. Nix, F. Mele, S. Jovic, B. F. Rodriguez, S. V. Gupta, F. Jin, G. Piumatti, G. L. Presti, A. F. Pellanda, M. Biggiogero, M. Tarkowski, M. S. Pizzuto, E. Cameroni, C. Havenar-Daughton, M. Smithey, D. Hong, V. Lepori, E. Albanese, A. Ceschi, E. Bernasconi, L. Elzi, P. Ferrari, C. Garzoni, A. Riva, G. Snell, F. Sallusto, K. Fink, H. W. Virgin, A. Lanzavecchia, D. Corti, D. Veesler, Mapping neutralizing and immunodominant sites on the SARS-CoV-2 spike receptor-binding domain by structure-guided high-resolution serology. *Cell* **183**, 1024–1042.e21 (2020).

37. A. J. Greaney, T. N. Starr, P. Gilchuk, S. J. Zost, E. Binshtein, A. N. Loes, S. K. Hilton, J. Huddleston, R. Eguia, K. H. D. Crawford, A. S. Dingens, R. S. Nargi, R. E. Sutton, N. Suryadevara, P. W. Rothlauf, Z. Liu, S. P. J. Whelan, R. H. Carnahan, J. E. Crowe, J. D. Bloom, Complete mapping of mutations to the SARS-CoV-2 spike receptor-binding domain that escape antibody recognition. *Cell Host Microbe* **29**, 44–57.e9 (2020).

38. K. W. Ng, N. Faulkner, G. H. Cornish, A. Rosa, R. Harvey, S. Hussain, R. Ulferts, C. Earl, A. G. Wrobel, D. J. Benton, C. Roustan, W. Bolland, R. Thompson, A. Agua-Doce, P. Hobson, J. Heaney, H. Rickman, S. Paraskevopoulou, C. F. Houlihan, K. Thomson, E. Sanchez, G. Y. Shin, M. J. Spyer, D. Joshi, N. O'Reilly, P. A. Walker, S. Kjaer, A. Riddell, C. Moore, B. R. Jebson, M. Wilkinson, L. R. Marshall, E. C. Rosser, A. Radziszewska, H. Peckham, C. Ciurtin, L. R. Wedderburn, R. Beale, C. Swanton, S. Gandhi, B. Stockinger, J. McCauley, S. J. Gamblin, L. E. McCoy, P. Cherepanov, E. Nastouli, G. Kassiotis, Preexisting and de novo humoral immunity to SARS-CoV-2 in humans. *Science* **370**, 1339–1343 (2020).

39. P. Nguyen-Contant, A. K. Embong, P. Kanagaiah, F. A. Chaves, H. Yang, A. R. Branche, D. J. Topham, M. Y. Sangster, S protein-reactive IgG and memory B cell production after human SARS-CoV-2 infection includes broad reactivity to the S2 subunit. *MBio* **11**, e01991-20 (2020).

40. A. Amitai, M. Sangesland, R. M. Barnes, D. Rohrer, N. Lonberg, D. Lingwood, A. K. Chakraborty, Defining and manipulating B cell immunodominance hierarchies to elicit broadly neutralizing antibody responses against influenza virus. *Cell Syst.* **11**, 573–588.e9 (2020).

41. R. Di Niro, S.-J. Lee, J. A. Vander Heiden, R. A. Elsner, N. Trivedi, J. M. Bannock, N. T. Gupta, S. H. Kleinstein, F. Vigneault, T. J. Gilbert, E. Meffre, S. J. McSorley, M. J. Shlomchik, Salmonella infection drives promiscuous B cell activation followed by extrafollicular affinity maturation. *Immunity* **43**, 120–131 (2015).

42. M. Kuraoka, A. G. Schmidt, T. Nojima, F. Feng, A. Watanabe, D. Kitamura, S. C. Harrison, T. B. Kepler, G. Kelsoe, Complex antigens drive permissive clonal selection in germinal centers. *Immunity* **44**, 542–552 (2016).

43. C. Havenar-Daughton, A. Sarkar, D. W. Kulp, L. Toy, X. Hu, I. Deresa, O. Kalyuzhniy, K. Kaushik, A. A. Upadhyay, S. Menis, E. Landais, L. Cao, J. K. Diedrich, S. Kumar, T. Schiffner, S. M. Reiss, G. Seumois, J. R. Yates, J. C. Paulson, S. E. Bosinger, I. A. Wilson, W. R. Schief, S. Crotty, The human naive B cell repertoire contains distinct subclasses for a germline-targeting HIV-1 vaccine immunogen. *Sci. Transl. Med.* **10**, eaat0381 (2018).

44. B. N. Bell, A. E. Powell, C. Rodriguez, J. R. Cochran, P. S. Kim, Neutralizing antibodies targeting the SARS-CoV-2 receptor binding domain isolated from a naïve human antibody library. *Protein Sci.* **30**, 716–727 (2021).

45. P. W. H. I. Parren, D. R. Burton, in *Advances in Immunology* (Academic Press, 2001), vol. 77, pp. 195–262.

46. C. G. Rappazzo, L. V. Tse, C. I. Kaku, D. Wrapp, M. Sakharkar, D. Huang, L. M. Deveau, T. J. Yockachonis, A. S. Herbert, M. B. Battles, C. M. O'Brien, M. E. Brown, J. C. Geoghegan, J. Belk, L. Peng, L. Yang, Y. Hou, T. D. Scobey, D. R. Burton, D. Nemazee, J. M. Dye, J. E. Voss, B. M. Gunn, J. S. McLellan, R. S. Baric, L. E. Gralinski, L. M. Walker, Broad and potent activity against SARS-like viruses by an engineered human monoclonal antibody. *Science* **371**, eabf4830 (2021).

47. L. R. Baden, H. M. El Sahly, B. Essink, K. Kotloff, S. Frey, R. Novak, D. Diemert, S. A. Spector, N. Rouphael, C. B. Creech, J. McGettigan, S. Khetan, N. Segall, J. Solis, A. Brosz, C. Fierro, H. Schwartz, K. Neuzil, L. Corey, P. Gilbert, H. Janes, D. Follmann, M. Marovich, J. Mascola, L. Polakowski, J. Ledgerwood, B. S. Graham, H. Bennett, R. Pajon, C. Knightly, B. Leav, W. Deng, H. Zhou, S. Han, M. Ivarsson, J. Miller, T. Zaks; COVE Study Group, Efficacy and Safety of the mRNA-1273 SARS-CoV-2 Vaccine. *N. Engl. J. Med.* **384**, 403–416 (2021).

48. D. M. Skowronski, G. De Serres, Safety and efficacy of the BNT162b2 mRNA covid-19 vaccine. *N. Engl. J. Med.* **384**, 1576–1577 (2021).

49. A. G. Schmidt, H. Xu, A. R. Khan, T. O'Donnell, S. Khurana, L. R. King, J. Manischewitz, H. Golding, P. Suphaphiphat, A. Carfi, E. C. Settembre, P. R. Dormitzer, T. B. Kepler, R. Zhang, M. A. Moody, B. F. Haynes, H.-X. Liao, D. E. Shaw, S. C. Harrison, Preconfiguration of the antigen-binding site during affinity maturation of a broadly neutralizing influenza virus antibody. *Proc. Natl. Acad. Sci. U.S.A.* **110**, 264–269 (2013).

50. M. Sangesland, A. S. Yousif, L. Ronsard, S. W. Kazer, A. L. Zhu, G. J. Gatter, M. R. Hayward, R. M. Barnes, M. Quirindongo-Crespo, D. Rohrer, N. Lonberg, D. Kwon, A. K. Shalek, D. Lingwood, A single human VH-gene allows for a broad-spectrum antibody response targeting bacterial lipopolysaccharides in the blood. *Cell Rep.* **32**, 108065 (2020).

51. J. J. Trombetta, D. Gennert, D. Lu, R. Satija, A. K. Shalek, A. Regev, Preparation of single-cell RNA-seq libraries for next generation sequencing. *Curr. Protoc. Mol. Biol.* **107**, 4.22.1–4.22.17 (2014).

52. A. P. Masella, A. K. Bartram, J. M. Truszkowski, D. G. Brown, J. D. Neufeld, PANDAseq: Paired-end assembler for illumina sequences. *BMC Bioinformatics* **13**, 31 (2012).

53. S. H. Scheres, RELION: Implementation of a Bayesian approach to cryo-EM structure determination. *J. Struct. Biol.* **180**, 519–530 (2012).

54. S. Q. Zheng, E. Palovcak, J. P. Armache, K. A. Verba, Y. Cheng, D. A. Agard, MotionCor2: Anisotropic correction of beam-induced motion for improved cryo-electron microscopy. *Nat. Methods* **14**, 331–332 (2017).

55. K. Zhang, GCTF: Real-time CTF determination and correction. *J. Struct. Biol.* **193**, 1–12 (2016).

56. T. Wagner, F. Merino, M. Stabrin, T. Moriya, C. Antoni, A. Apelbaum, P. Hagel, O. Sitsel, T. Raisch, D. Prumbaum, D. Quentin, D. Roderer, S. Tacke, B. Siebolds, E. Schubert, T. R. Shaikh, P. Lill, C. Gatsogiannis, S. Raunser, SPHIRE-crYOLO is a fast and accurate fully automated particle picker for cryo-EM. *Commun. Biol.* **2**, 218 (2019).

57. A. Punjani, J. L. Rubinstein, D. J. Fleet, M. A. Brubaker, cryoSPARC: Algorithms for rapid unsupervised cryo-EM structure determination. *Nat. Methods* **14**, 290–296 (2017).

58. E. F. Pettersen, T. D. Goddard, C. C. Huang, G. S. Couch, D. M. Greenblatt, E. C. Meng, T. E. Ferrin, UCSF Chimera—A visualization system for exploratory research and analysis. *J. Comput. Chem.* **25**, 1605–1612 (2004).

59. P. Emsley, K. Cowtan, Coot: Model-building tools for molecular graphics. *Acta Crystallogr. D Biol. Crystallogr.* **60**, 2126–2132 (2004).

60. J. Mata-Fink, B. Kriegsman, H. X. Yu, H. Zhu, M. C. Hanson, D. J. Irvine, K. D. Wittrup, Rapid conformational epitope mapping of anti-gp120 antibodies with a designed mutant panel displayed on yeast. *J. Mol. Biol.* **425**, 444–456 (2013).

Naive human B cells engage the receptor binding domain of SARS-CoV-2, variants of concern, and related sarbecoviruses

Jared FeldmanJulia BalsClara G. AltomareKerri St. DenisEvan C. LamBlake M. HauserLarance RonsardMaya SangeslandThalia Bracamonte MorenoVintus OkonkwoNathania HartojoAlejandro B. BalazsGoran BajicDaniel LingwoodAaron G. Schmidt

Preexisting immunity against SARS-CoV-2

The development of protective humoral immune responses after infection or vaccination depends on the recruitment, activation, and maturation of naive B cells. The specificity of the naive B cell repertoire for SARS-CoV-2 in uninfected individuals is unknown. Feldman *et al*. performed B cell receptor (BCR) sequencing in naive B cells targeting the receptor binding domain (RBD) of SARS-CoV-2 from seronegative donors. RBD-specific naive B cells were identified across all donors, and recombinant antibodies generated from these BCR sequences bound with affinity to the RBD of SARS-CoV-2 and variants of concern. Furthermore, these naive and affinity-matured antibodies were able to neutralize SARS-CoV-2. These findings suggest that RBD-specific naive B cell precursors are present across the human population, which may be informative for future vaccine design.

View the article online
https://www.science.org/doi/10.1126/sciimmunol.abl5842
Permissions
https://www.science.org/help/reprints-and-permissions

Use of think article is subject to the Terms of service